NJC

New Journal of Chemistry

A journal for new directions in chemistry

Accepted Manuscript

This article can be cited before page numbers have been issued, to do this please use: S. M. Wagalgave, S. D. Padghan, M. Al Kobaisi, D. D. La, K. Bhamidipati, N. Puvvada, R. S. Bhosale, S. V. Bhosale and S. Bhosale, *New J. Chem.*, 2020, DOI: 10.1039/D0NJ01235A.

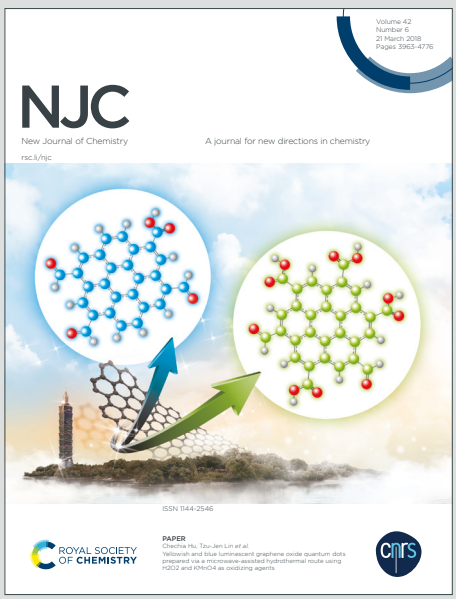

This is an Accepted Manuscript, which has been through the Royal Society of Chemistry peer review process and has been accepted for publication.

Accepted Manuscripts are published online shortly after acceptance, before technical editing, formatting and proof reading. Using this free service, authors can make their results available to the community, in citable form, before we publish the edited article. We will replace this Accepted Manuscript with the edited and formatted Advance Article as soon as it is available.

You can find more information about Accepted Manuscripts in the Information for Authors.

Please note that technical editing may introduce minor changes to the text and/or graphics, which may alter content. The journal's standard Terms & Conditions and the Ethical guidelines still apply. In no event shall the Royal Society of Chemistry be held responsible for any errors or omissions in this Accepted Manuscript or any consequences arising from the use of any information it contains.

View Article Online
DOI: 10.1039/D0NJ01235A

ARTICLE

Selectivity and bio-compatibility of self-assembled chiral flower-like and helical nanostructures

Received 00th January 20xx,
Accepted 00th January 20xx

DOI: 10.1039/x0xx00000x

Sopan M. Wagalgave,[a,f] Sachin D. Padghan,[a] Mohammad Al Kobaisi,[c] Duong Duc La,[d] Keerti Bhamidipati,[f,g] Nagaprasad Puvvada,[f,g] Rajesh S. Bhosale,[e] Sidhanath V. Bhosale,[a,f*] Sheshanath V. Bhosale[b*]

The molecular building block NDI-LCA was synthesized by substitution of NDA at di-imide position with two lithocholic acid moieties. It was found that the NDI-LCA conjugate exhibits good thermal stability. The photophysical such as UV-vis and fluorescence spectral measurements and theoretical calculations reveal that NDI-LCA possesses stronger absorption and fluorescence emission properties. Furthermore, NDI-LCA derivative self-assembled into chiral flower-like structures in THF/MCH solvent mixture, whereas, NDI-LCA in THF/water produces chiral fibril nanostructures. The formation of supramolecular self-assembly in solution was characterization by UV-vis, fluorescence spectroscopy, and dynamic light scattering (DLS). Circular dichroism is used to study chiral induction in supramolecular structures. Scanning Electron Microscopy (SEM) confirms the formed structure on the silicon wafer. X-ray diffraction (XRD) clearly shows the formation of the crystalline nature of morphology. In addition, NDI-LCA's supramolecular structures in THF exhibit remarkable bio-compatibility and increased cellular uptake in cancer cells. From cell morphology and uptake studies, it can be assumed that NDI-LCA in THF supramolecular structures can act effectively as a platform for both cell markers and as a delivery agent for further studies.

1. Introduction

The self-assembly of chiral synthons is driven by non-covalent interactions such as hydrogen bonding, hydrophobic forces, van der Waals and π-π interactions.[1] These forces regulate the supramolecular chirality in self-assembled structures.[2] The chiral assemblies are fundamentally important to understand the relationship between molecular structures and supramolecular assemblies and mimic the biological self-assembly.[3-6] It is well documented that chiral flower-shaped morphologies such as rose-, chrysanthemum-, peony- and dandelion-like were fabricated *via* microwave heating or a hydrothermal method.[7-13] These methods are mainly based on the self-assembly of small organic molecules, peptides, and amphiphiles with various inorganic materials as well as pure organic building blocks such as a polymer, DNA, aminoglycoside antibiotics.[14-18] The chirality of supramolecular nanoflowers is defined by optical activity (OA).[19,20] Chiral flowers like nanostructures are rarely been reported in pure organic solvents.[21-25] The chiral assemblies exhibit potential applications in molecular recognition, asymmetric catalysis, chiral separation, medicine, tissue engineering, and optoelectronic materials.[26-31] However, it remains the challenging issue to fabricate the controlled chiral nanoflowers and the transformation of molecular chirality during such assembly process.[21,22,24,32]

Bile acids are biologically important surfactants and are synthesized in the liver.[33]The molecular structure of bile acids is different than that of conventional surfactants. They exhibit a hydrophobic convex side and hydrophilic concave side and are called as facial amphiphiles.[34] Lithocholic acid (LCA) is a secondary bile acid category. The literature search revealed that researchers have shown the self-assembly of LCA leads to the formation of primary micelles, helical ribbons, nanotubes, tubular spherulites, fan-like bundles, spiral tubes, monodispersed nanotubes, and hydrogel and.[35] The fabrication of these nanostructures mainly depends on the self-assembly conditions.[36] Due to the self-assembly nature of lithocholic acid these nanostructures may exhibit structural rigidity, bio-compatibility, bio-degradability, and selectivity towards cancer cell lines and are thus, considered important for its potential application in drug delivery.

[a.] Polymers and Functional Materials Division, CSIR-Indian Institute of Chemical Technology, Hyderabad 500007, Telangana, India.
[b.] School of Chemical Sciences, Goa University, Taleigao Plateau, Goa 403206, India. svbhosale@unigoa.ac.in
[c.] School of Science, Faculty of Science, Engineering and Technology, Swinburne University of Technology, Hawthorn, Australia.
[d.] Institute of Chemistry and Materials, Hoang Sam, Hanoi, Vietnam.
[e.] Department of Chemistry, Indrashil University, Kadi, Mehsana-382740, Gujarat, India
[f.] Applied Biology Division, CSIR-Indian Institute of Chemical Technology, Hyderabad 500007, Telangana, India.
[g.] Academy of Scientific and Innovative Research (AcSIR), Ghaziabad-201002, India. bhosale@iict.res.in

† Footnotes relating to the title and/or authors should appear here.
Electronic Supplementary Information (ESI) available: [details of any supplementary information available should be included here]. See

View Article Online
DOI: 10.1039/D0NJ01275A

Naphthalene diimide (NDI) is a rylene dye. NDI is a planar n-type semiconductor molecule.[37] Recent studies have shown the self-assembly of NDI strongly depends on the substituents present on its imide/core positions. It has been shown that NDIs and their derivatives can self-assemble into chiral assemblies, such as helical fibers, helical nanotubes, helical ribbons, by varying the external stimuli as well as the subunits connecting at its imide/core positions.[38] Ghosh *et al* reported that self-assembly NDI-amphiphiles showed a high impact on antimicrobial activity.[38] Very recently, we have shown the self-assembly of NDI-cholic acid (NDI-CA) and NDI-deoxycholic acid (NDI-DCA) conjugates,[39] our finding revealed that NDI-DCA self-assemble into the super-helix structure in THF: water mixes, however, and NDI-DA does not produce any decent assemblies. Inspired by these results, we sought to apply LCA conjugated NDI nanoengineered materials and check their selectivity for application in drug delivery and biomedical research to avoid the off-target toxicity of various drugs.

In this work, we investigate the effect of LCA substituents on the self-assembly of NDI-LCA in both polar and non-polar solvent systems such as THF: H_2O and THF: MCH, respectively. Interestingly, NDI-LCA produces a 3D chiral globular flower-like morphology in THF: MCH, however in a polar solvent (THF: H_2O), the NDI-LCA conjugate exhibits fibril network. The CD spectral study displays the chiral behavior of the supramolecular nano-architecture. We believe that the H-bonding along with π-π interaction within the NDI core plays an important role in supramolecular assemblies. This study may show the way to stimulate the change in supramolecular architectures by simply manipulating the solvent system from non-polar to polar. Further, we performed *In* vitro studies to elucidate the biocompatibility and selective cellular uptake properties in cancerous cells.

2. Experimental Section

2.1. General Materials and Methods

Chemical reagents were purchased and used as received. All are air- and water-sensitive reactions were performed under nitrogen atmosphere. Thin-layer chromatography (TLC) (Merck Co.) was performed using 0.25 mm thick plates pre-coated with silica gel (40–60 mm, F254) and visualized using UV light (254 and 365 nm). NMR spectra were recorded with a 300 MHz on Bruker spectrometer using DMSO-d_6 as solvent and tetramethylsilane as an internal standard. IR spectra were recorded on a Thermo Nicolet Nexus 670 FR-IR spectrometer in the form of non-hygroscopic KBr pellets. ESI-MS data were taken on Shimadzu lab solutions. High-resolution mass spectra (HRMS), atmospheric-pressure chemical ionization (APCI) experiments were carried out on FTMS, ionizing by APCI from an atmospheric solids analysis probe (ASAP). MALDI-TOF measurements, a Shimadzu Biotech Axima performance spectroscopic instrument was used.

UV-vis absorption spectra were measured on a Shimadzu UV-1800 spectrophotometer at room temperature. Fluorescence emission spectra were recorded on an RF-6000 (Shimadzu, Japan) spectrofluorophotometer. All experiments were performed in a quartz cell with a 1 cm path length with a 360 nm excitation wavelength. DLS measurements were conducted using a Brookhaven Instrument Corp., 90Plus Particle Size equipped with a He–Ne laser (632.8 nm, 35 mW), and quartz cuvette.

2.2. Synthesis

Synthesis of (R,R,R,S,R,R,S,S,4R,4'R)-N,N'-((1,3,6,8-tetraoxobenzo[lmn][3,8]phenanthroline-2,7(1H,3H,6H,8H)-diyl)bis(ethane-2,1-diyl))bis(4-((3R,5R,8R,9S,10S,13R,14S,17R)-3-hydroxy-10,13-dimethylhexadecahydro-1H-cyclopenta[a]phenanthren-17-yl)pentanamide) (NDI-LCA). Lithocholic acid 232 mg (0.62 mmol), hydroxy-benzotriazole (HOBt) 167 mg (1.2 mmol) and 1-ethyl-3-(3-dimethylaminopropyl)carbodiimide [EDCI] 239 mg (1.2 mmol) were dissolved in dry DMF. After stirring at 0 °C for 30 min, NDI-amine 100 mg (0.28 mmol) was added and the resulting reaction mixture was stirred at ambient temperature for further 24 h. The completion of reaction was monitored using TLC. The reaction mixture was poured in to crushed ice, white precipitate was formed. The precipitate was filtered and the obtained crude product was purified by column chromatography on neutral Al_2O_3 (2% MeOH/CH_2Cl_2). The compound was isolated as white solid, 118 mg, yield 38%. ^{1}H NMR (DMSO-d_6, 300 MHz):δ 8.68 (s, 4H; Ar-H) 7.89 (s, 2H; NH) 4.45 (d, J = 4.40 Hz, 2H) 4.16 (t, *J* = 5.50 Hz, 4H) 1.93- 0.85 (m, 66H) 0.73 (s, 6H; CH_3) 0.48 (s, 6H; CH_3);IR (KBr, cm^{-1}):770, 1188, 1245, 1341, 1400, 1581, 1660, 2930, 3160, 3410; ESI-MS (m/z %): 1070 (100) $[M+H]^+$; MALDI-TOF: 1092.27 $[M+Na]^+$.

Sample Preparation. A stock solution of NDI-LCA (ca. = 1×10^{-4} M) was prepared in THF. A 0.2 mL aliquot of this stock solution was transferred in separate volumetric flasks and equilibrate with the different ration of MCH and H_2O and made up to 2 mL volume with respective solvents. The obtained solutions were allowed to equilibrate for 2h before the spectroscopic as well as morphology measurements.

2.3. Spectroscopic and morphology experiments

2.3.1 UV-vis absorption measurements. UV-vis absorption measurements were performed on UV-vis-1800 Shimadzu spectrometer using a 1 cm path length quartz cuvette. A 0.2 mL aliquot of NDI-LCA (1×10^{-3} M stock solution) was transferred to a vial and made up to a final volume of 3 mL. The solutions were allowed to equilibrate for 2h before their spectral measurements.

2.3.2 Fluorescence measurements. Fluorescence spectra measurements were carried out on an RF-6000 (Shimadzu, Japan) spectrofluorophotometer. The measurements were performed at room temperature in a 1 cm path length quartz cell with an excitation wavelength of λ_{ex} = 360.

2.3.3. Circular Dichroism (CD).CD spectra were recorded on an AVIV 202 CD spectrometer under a nitrogen atmosphere. The measurements were performed in a quartz cuvette with a 1 mm path length. A 0.2 mL aliquot of NDI-LCA (1×10^{-3} M stock

View Article Online
DOI: 10.1039/D0NJ01275A

solution) was transferred to a vial and made up to a final volume of 3 mL in suitable solvents and allowed to equilibrate for 2 h then CD spectra recorded.

2.3.4. Scanning electron microscopy measurements (SEM). Firstly, the silicon wafer substrate was cleaned by rinsing in acetone and ethanol then Milli Q water. Then the sample sputter was coated with gold for 10 s at 0.016 mA Ar plasma (SPI, West Chester, USA) using an FEI Nova NanoSEM (Hillsboro, USA) operating at high vacuum which provided direct visualization of the self-assembled material. The samples were prepared by solvent evaporation.

2.3.5. Dynamic light scattering measurements (DLS). This experiment was performed using a Brookhaven Instrument Corp., 90 Plus Particle Size equipped with a He–Ne laser (632.8 nm, 35 mW), and quartz cuvette.

2.3.6. X-ray diffraction (XRD) measurements. The self-assembled NDI-LCA in the THF: MCH and THF: H_2O solvent mixtures were used for XRD measurements. Then precipitates of NDI-LCA were dropped on the silicon wafer and dried at 40 ^oC for 4 h, this process was repeated for 3 times. Structure and crystallinity were analyzed on an X'Pert PRO PANalytical machine with a 0.15405 nm Cu-K_α radiation source.

2.3.7. Infrared spectroscopy (IR) measurements. FT-IR spectra were measured on a PerkinElmer spectrometer. The liquid sample in THF: MCH and THF: H_2O were drop-casted and the solvent was allowed to evaporate on the surface naturally.

2.3.8. Molecular modeling. Density functional theory (DFT) and TD-DFT calculations with no consideration of dispersion interactions in the gas phase were conducted using ORCA 4.0 suite of programs.

2.3.9. Cell Culture. Cancerous cells Neuro-2a (Murine neuroblastoma cell line) were obtained from the National Centre for Cell Sciences (NCCS), Pune, India. The cells were then cultured in DMEM (Dulbecco Modified Eagle Medium) media (Gibco) supplemented with 10% (v/v) foetal bovine serum, 1% L-glutamine, 1% non-essential amino acid, 1%penicillin, and 1% streptomycin. All cells were then maintained in a humidified 5% CO2 incubator at 37 °C

2.3.10. Cytotoxicity studies using MTT assay. The cell cytotoxicity of NDI-LCA and NDI was carried out using MTT (3-(4,5-dimethylthiazole-2-yl)-2,5–diphenyltetrazolium bromide reagent) assay in Neuro-2a murine cancerous cells as described previously with minor modification.[47, 48] Cells were seeded and grown in 96-well plates separately for 24 h at 1 × 10^4 cells per well and then treated in triplicates at different concentrations (6.25, 12.5, 25 and 50 µg/100µl). The cells were then washed twice with 1 × PBS and further incubated with 450 µl (1g/ml) of MTT solution at 37 °C for 3–4 h. Later, MTT solubilizing buffer was used to dissolve the formazan crystals and absorbance was recorded at 570nm by using a Multimode microplate reader (Varioskan, Thermo Fisher Scientific).

2.3.11. Intra-cellular uptake and morphology study using confocal microscopy. The cellular uptake efficiency and the cytoplasmic distribution of NDI-LCA and NDI (ESI†, Scheme S1) was done in Neuro-2a murine cancerous cells. The cells were seeded (5 x 10^4) on 35mm cover glass with 1 ml of growth medium and grown at 37 °C. The cells were then treated with NDI-LCA and NDI (ESI†, Scheme S1) and stained with commercially available LysoTracker Red (LTR) as per manufacturer's protocol at 3, 6, and 24 h time points with a concentration of 10 µg/100µl. After that, the cells were washed with 1 × PBS twice and fixed using 4% formaldehyde solution. The cells were then washed again with a 1 × PBS solution twice to remove the excess formaldehyde solution and mounted on a microscopic slide using Fluoroshield mounting solution. The fluorescent images were then captured using a confocal microscope (Nikon Ti Eclipse Tokyo, Japan) at 60 X magnification and with 2.5 X zoom.

3. Results and Discussion

3.1. Synthesis

The NDI-LCA was synthesized starting from naphthalenedianhydride (NDA): At first step, NDA was treated with mono-boc protected ethylenediamine to yield the compound **1**. Compound **1** was treated with TFA in dichloromethane (DCM) at room temperature to yield NDI-diamine **2**.[40] Amide coupling of NDI-diamine **2**with LCA in the presence of EDC and catalytic HOBt resulted in NDI-LCA in 38% yield (Scheme 1).

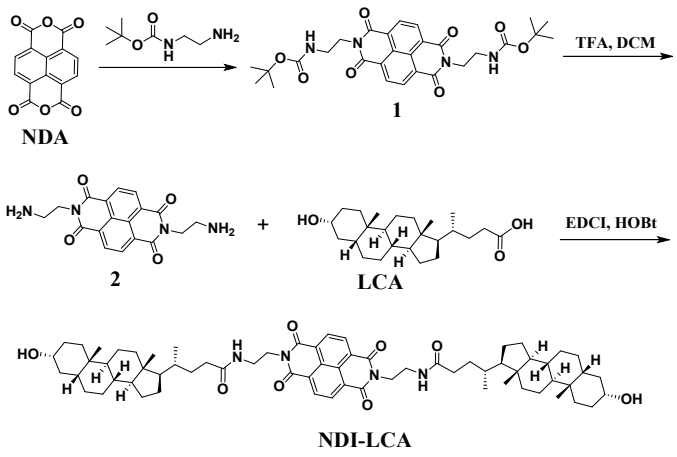

Scheme 1. Synthesis of NDI-LCA conjugates.

3.2. Thermal Properties

The thermal properties of NDI-LCA were investigated by thermogravimetric analysis (TGA) under a nitrogen flow. The results are illustrated in Fig. 1. For 5% weight loss, NDI-LCA exhibits decomposition temperature (T_d) over 330 ^oC. This indicates NDI-LCA is thermally stable.

View Article Online
DOI: 10.1039/D0NJ01235A

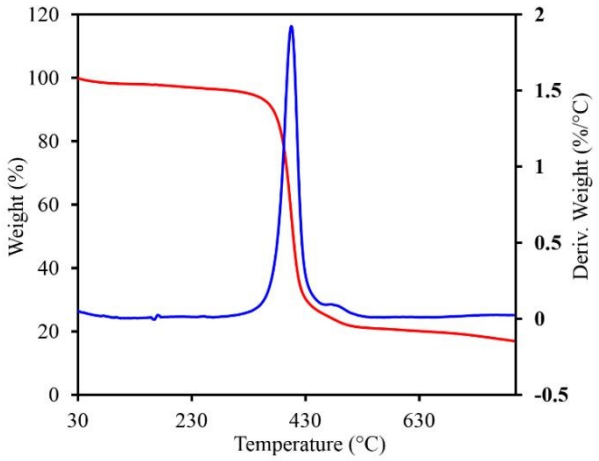

Fig. 1 Thermogravimetric analysis of NDI-LCA.

3.3. UV-vis properties

UV-vis spectroscopy of NDI-LCA was performed in different solvent systems to investigate their respective absorbance properties. As illustrated in Fig. 2a, the UV-vis spectrum of NDI-LCA in pure THF produces two main absorption peaks at 359 nm and 379 nm along with a shoulder peak at around 341 nm. The absorption maxima peaks are attributed to π-π* transitions. With the addition of MCH (0-95%), the absorbance peak intensities were decreased with increasing MCH concentration. Particularly upon the addition of MCH (80%), the UV-vis absorption peak intensity significantly decreased. Moreover, the addition of 90 and 95% MCH exhibits a small bathochromic shift of the absorption bands to 362 and 383 nm, indicating *J*–type of aggregation (Fig. 2a). The UV-vis absorption of NDI-LCA in THF/H_2O mixture is shown in Fig. 2b. The addition of H_2O (0-60%) shows a slight decrease in absorption peak intensity as compared to 70% H_2O in THF. However, further, an increase in H_2O volume to 80-90%, absorption peak appeared at 361 nm and 381 nm with absorption band shift to 371 nm and 385 nm, with shifts are about 11 and 6 nm, respectively as compared with NDI-LCA in THF. Further NDIA-LCA in 95% water/THF, absorption gives an additional shift of 4 nm i.e. bands appeared at 365 nm and 385, suggesting *J*-type of aggregation. Herein, we presume that the change in aggregation mode due to an increase in solubility of LCA subunits in H_2O.

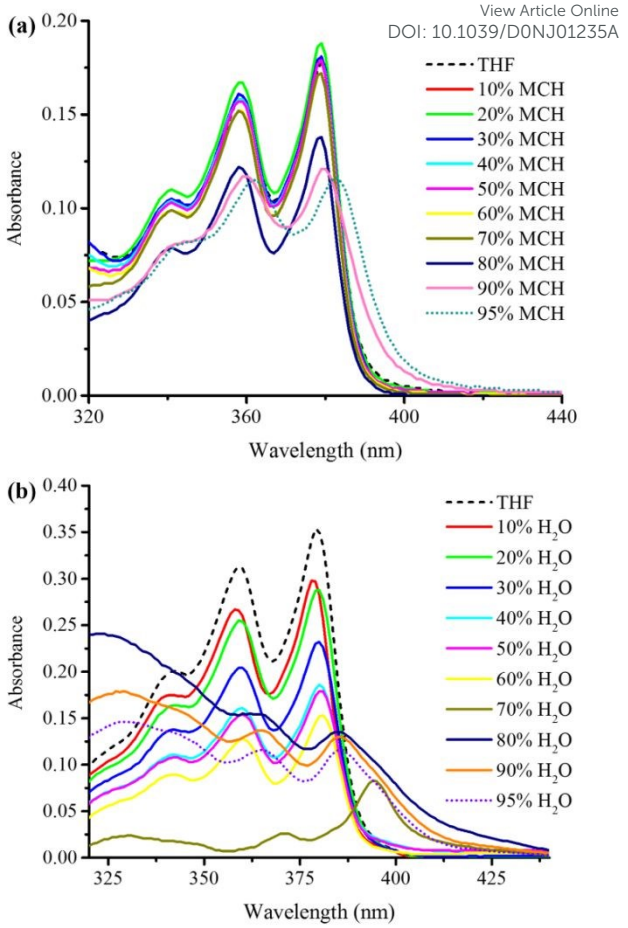

Fig. 2 UV-vis absorption spectra of NDI-LCA in (a) THF and THF: MCH (0-95%) and (b) in THF and THF: H_2O (0-95%).

3.4. Fluorescence Properties

Fluorescence emission spectroscopy technique was employed to investigate the intermolecular interaction of NDI-LCA in different solvent systems. As shown in Fig. 3a, NDI-LCA in THF exhibited two intense peaks at around 408 nm and 430 nm, upon excitation at 360 nm. With the addition of MCH (0-95%) volume, the fluorescence of NDI-LCA decreased due to the aggregation caused by quenching (ACQ). It is notable that the fluorescence peak significantly decreased with a blue shift to 401 nm and 426 nm in presence of 95% MCH. The shift of emission peak was ascribed to the formation of π-π stacks within the NDI cores. A similar quenching effect was observed in THF/H_2O (0-95%). It indicates, in presence of a large volume of H_2O, the LCA hydrophilic facial end goes outward and hydrophobic interaction between two LCA subunits becomes stronger along with π-π stacking interaction between NDI moieties.

The fluorescence quantum yield (Φ_F) of NDI-LCA was measured in THF, THF/MCH (5:95, v/v), and THF/water (5:95, v/v) were calculated using quinine sulfate standard reference dye, the quantum yield of NDI-LCA upon excitation at 360 nm was found to be 4.63% in THF. However, in THF/MCH and THF/water at the ratio 5:95 v/v, reduction of the quantum yield was observed i.e. 0.08 and 0.003, respectively.[41]

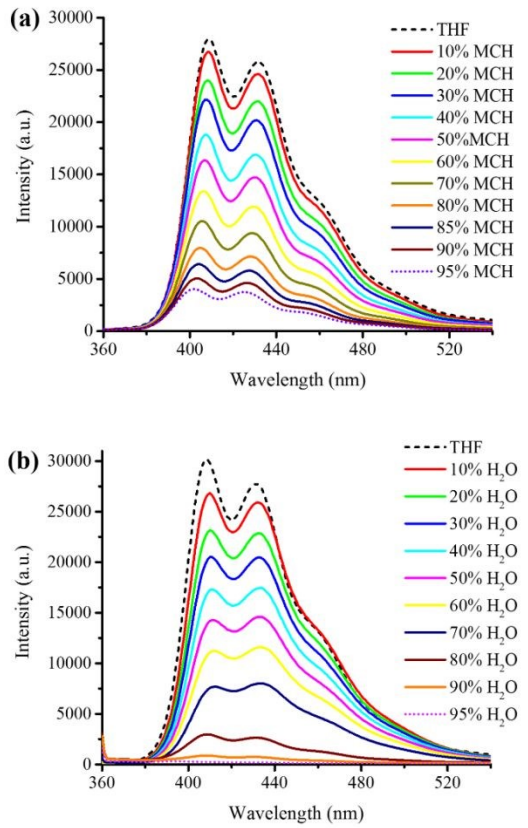

Fig. 3 Fluorescence emission spectra of NDI-LCA in (a) THF and THF: MCH (0-95%) and (b) in THF and THF: H_2O (0-95%).

3.5. Scanning electron microscopy (SEM) measurements

Scanning electron microscopy (SEM) was employed to visualize the self-assembled structures of NDI-LCA in THF/MCH with varying concentration of MCH as shown in Fig. 4, Fig. 5 and Fig.S5 and Fig. S6, which revealed distinctive micro-nano structures at 20 and 30 $f_{THF/MCH}$ volume fractions. At 20% $f_{THF/MCH}$flower-like microstructures were produced about 10 µM in length and 5 µM in width, these dimensions increased 15 µM and 10 µM in 30%$f_{THF/MCH}$, respectively. Knowing that the THF is the good solvent and MCH is the non-polar solvent, a higher solvophobic effect can be observed at lower $f_{THF/MCH}$, resulting in nucleation, and more numerous smaller microstructures at 20% $f_{THF/MCH}$ while increasing the $f_{THF/MCH}$to 30% allows for better solubility later nucleation and longer time for microstructure growth during solvent evaporation resulting in larger three-dimensional (3D) microstructures. The basic nanostructure of the flower-like microstructure at both $f_{THF/MCH}$is very similar, multi-layered curved sheets few tens of nanometers in thickness giving a porous microstructure, evidence for the kinetic control on the overall microstructure size using the same process of self-assembly.

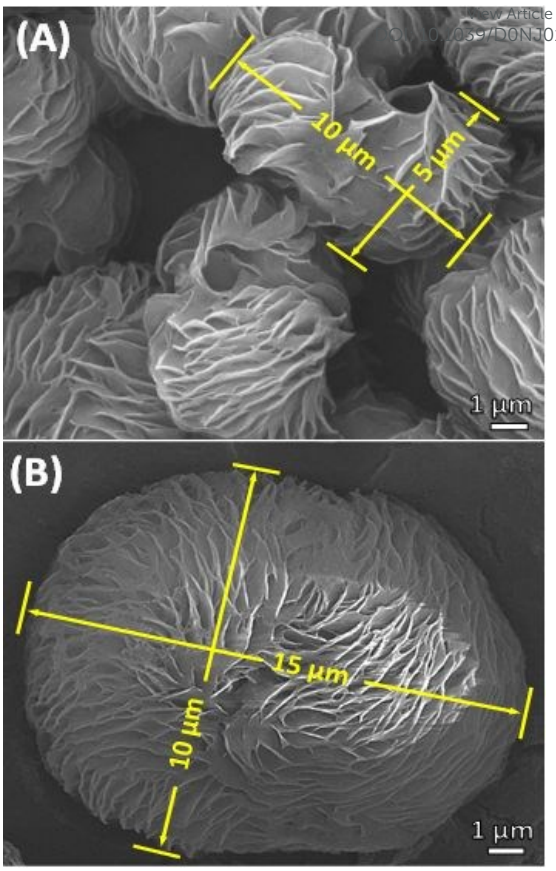

Fig. 4 SEM micrograph of the microstructures of self-assembled NDI-LCA in THF:MCH: (a) 2:8, and (b) 3:7 volumetric ratio after solvent evaporation, respectively.

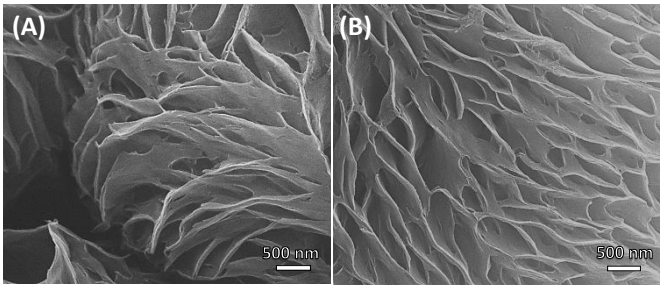

Fig. 5 ZoomedSEM image of the microstructures of self-assembled NDI-LCA in THF:MCH (a) 2:8, and (b) 3:7 volumetric ratio after solvent evaporation.

Further, SEM images of the NDI-LCA in THF: H_2O for 30:70% and 20:80% *v/v* ratio show in ESI Figure S7 and S8, respectively. The self-assembled morphology of NDI-LCA (30:70% *v/v* ratio) was composed of helical nanostructures with several micrometers in lengths and with diameters that range from 1 to 1.5 µM with wright handed-helical structures, which shown by a red arrow within the Figure 6. Further, the right-handed chirality of the self-assembled structure was confirmed using CD spectra (Fig. 8). Nevertheless, NDI-LCA in THF: H_2O (20:80% *v/v* ratio) resulted in nanofiber morphology with embedded nanoparticles. As H_2O% increases the helical nanofibers flattened. Thus, an increase in polarity of solvent in THF: H_2O causes loss of chirality in self-assembled materials.

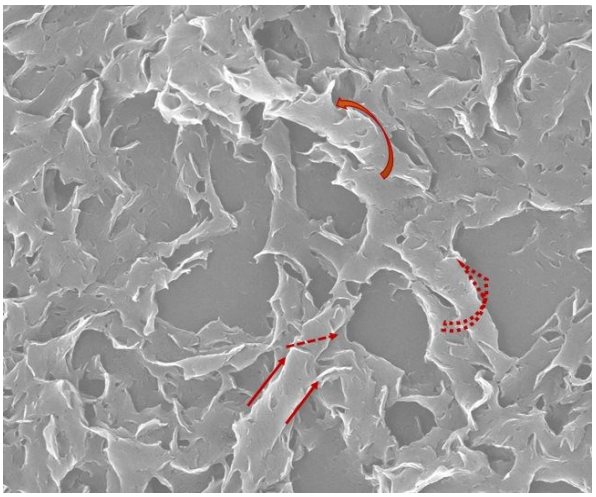

Fig.6 SEM micrograph of the microstructures of self-assembled NDI-LCA in THF:H_2O (3:7 volumetric ratio) after solvent evaporation. Arrow indicate mode of chirality.

3.6. Dynamic light scattering properties

Dynamic light scattering (DLS) was carried out to investigate the self-assembly of NDI-LCA in solution. The DLS results of NDI-LCA in THF: MCH and THF: H_2O are illustrated in Fig. S9a and Fig. S9b (ESI), respectively. The initial DLS measurement of NDI-LCA in THF shows a hydrodynamic diameter around 8.2 nm, indicating in pure THF, NDI-LCA does not form any aggregates. With the addition of MCH (*f* = 70%), NDI-LCAaggregatesexhibit the hydrodynamic diameter of 203.3 nm (Fig. S9a). Further addition of the MCH (*f* = 80%) has increased the hydrodynamic diameter to 417.7 nm Fig. S9a. Thus, an increase in MCH volume ration in THF displays an increase in the size of the NDI-LCA aggregates. Importantly, we performed the DLS measurements of NDI-LCA in THF and THF: H_2O solvent mixtures. The NDI-LCA in THF: H_2O (30:70%, v/v ratio) showed aggregates with a hydrodynamic diameter of 216 nm, whereas in THF: H_2O (20:80%, v/v ratio) exhibit an average hydrodynamic diameter of 414.4 nm. Thus the increase in H_2O volume increased in the size of the aggregates. We observed that the size of the NDI-LCA aggregates in THF: MCH and THF: H_2O are much smaller than the flower-like helical structures observed in SEM (Fig.5, Fig. 6 and ESI Fig. S5, S6, Fig. S7 and Fig. S8) microscopy, indicating that the larger growth of the formation of the microstructure takes place while solvent evaporation.

3.7. X-ray diffraction (XRD) properties

The XRD measurements were employed to investigate the crystallinity of NDI-LCA monomers, NDI-LCA aggregates in THF/H_2O, and THF/MCH mixtures. The XRD result is shown in Fig. S11. It can be seen that monomeric NDI-LCA molecules show an amorphous nature. However, when self-assembled in THF/MCH mixtures, the NDI-LCA aggregates exhibit the crystallinity in nature and the peaks are assigned 2θ = 12.5, 14.9 (more intense), 18, 19, and broad peak at 22. The XRD results indicate NDI-LCA in THF/MCH represents both the crystalline and amorphous nature. Whereas, in THF/H_2O, the 2θ= 22NDI-LCA exhibited in amorphous form. The NDI-LCA aggregates formed in THF/MCH mixture reveals higher crystallinity than that of obtained in THF/H_2O solution. This results is consistent with morphologies observed in above SEM images.

View Article Online
DOI: 10.1039/D0NJ01375A

3.8. Infrared (IR)spectroscopy

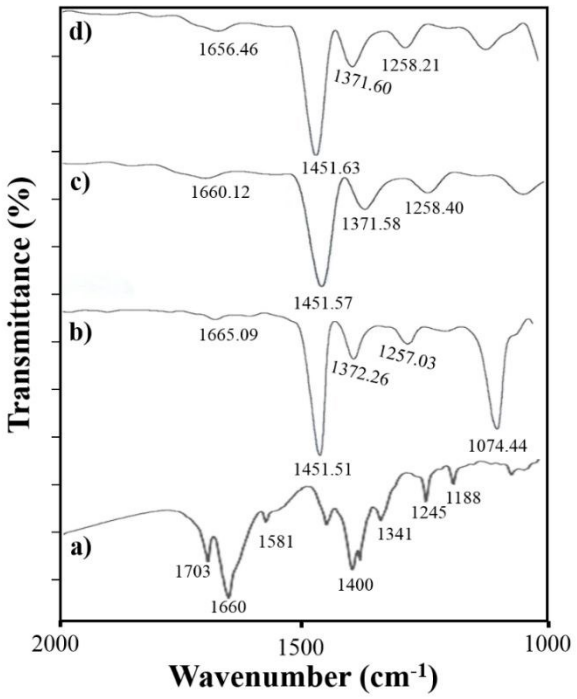

Fig.7 FT-IR transmission spectra of NDI-LCA in (a) THF, (b) THF:MCH (3:7, *v/v* ratio), (c) THF:MCH (20:80, *v/v* ratio); (d) THF:MCH (10:90, *v/v* ratio).

Fig.7 shows IR spectra of NDI-LCA in THF, THF:MCH (30:70, *v/v* ratio), THF:MCH (20:80, *v/v* ratio) and THF:MCH (10:90, *v/v* ratio). As shown in Fig. 7a, the transmission peaks appeared at about 1703 cm^{-1} and 1660 cm^{-1} are assigned to C=O stretching vibration of imide and amide functional moieties of NDI-LCA, respectively. With the 70% MCH addition to THF solution of NDI-LCA, the transmission peak at 1703 cm^{-1} disappeared and the peak at 1660 cm^{-1} was shifted to 1665 cm^{-1} with a decrease in intensity (Fig.7 b). As shown in Fig. 7c, the addition of MCH (*f* = 90%) resulted in the appearance of an amide C=O peak at 1656 cm^{-1}. The disappearance of IR transmission peak at 1703 cm^{-1} and change in amide C=O stretching peak position is ascribed to the hydrogen bonding interactions at the self-assembly process. We performed FT-IR measurements of NDI-LCA in THF and THF:H_2O solvent mixture system and are illustrated in Fig. S11a,b,c and d (ESI). With the addition of H_2O to the THF solution of NDI-LCA yields the disappearance of peak at 1703 cm^{-1}, whereas, the peak at 1660 cm^{-1} was shifted to 1642 cm^{-1}(Fig. S11 b), 1640 cm^{-1} (Fig. S11 c) and 1639 cm^{-1} (Fig. S11 d) in THF:H_2O volume ratio of 30:70, 20:80, 10:90, respectively. FT-IR experimental results indicate that amide hydrogen bonding is involved during self-assembly formation.

View Article Online
DOI: 10.1039/D0NJ01235A

3.9. Circular dichroism

Circular dichroism (CD) spectra were employed to further investigate the induction of chirality in THF, THF:MCH and THF:H_2O solvent systems. As illustrated in Fig. 8a, NDI-LCA in THF does not show any Cotton effect, suggesting the molecular chirality is absent in solvent through several chiral centers are present in LCA. With the addition of 50% MCH to NDI-LCA in THF solution display no change in the Cotton effect. Further addition of MCH (70%) exhibited a strong negative Cotton effect at 360 nm and 380 nm and positive Cotton effect at 345 nm, which was assigned to the transfer of molecular chirality in supramolecular structures. Moreover, the addition of 80% MCH shows intense negative Cotton effect signals at 360 nm and 380 nm and +ve signal at 335 nm with the similar shape of the CD, indicating chirality was perfectly maintained. We observed that the CD signal intensity increased with increasing the MCH content due to the increasing density and packing of the petals. The CD peaks can be attributed to the chiral stacking of NDI-LCA in flower-like morphologies. Hence, we believe that the flower-like structures obtained in THF:MCH (30% and 20% $f_{THF/MCH}$) could be recognized as chiral. Whereas, upon an increase in MCH content to 90% show decrease in Cotton effect intensity at 360 nm and 380 nm and disappearance of +ve Cotton signal at 345 nm, it may be due to larger supramolecular structures precipitate from the solution.

Fig. 8b provides the CD spectrum of the NDI-LCA sample in THF and THF:H_2O. In THF and 50% H_2O in THF, NDI-LCA does not exhibit an intense Cotton effect, indicating NDI-LCA material is achiral. With the addition of 70% MCH, we observed +ve Cotton effect at 345 nm and 405 nm along with strong -ve Cotton effect peaks at 360 nm and 380 nm, which confirms chirality mode is a right-handed helical structure and perfectly matches with SEM images shown in Figure 6. It is interesting to note that with the addition of 80% H_2O, the CD signals disappeared, indicating nanostructure loses the chirality. The CD inactive and nanostructures obtained by SEMS also confirm non-helical structures (Fig. S8). Thus the volume of MCH and H_2O in THF plays an important role in to induce chirality in the supramolecular structures.

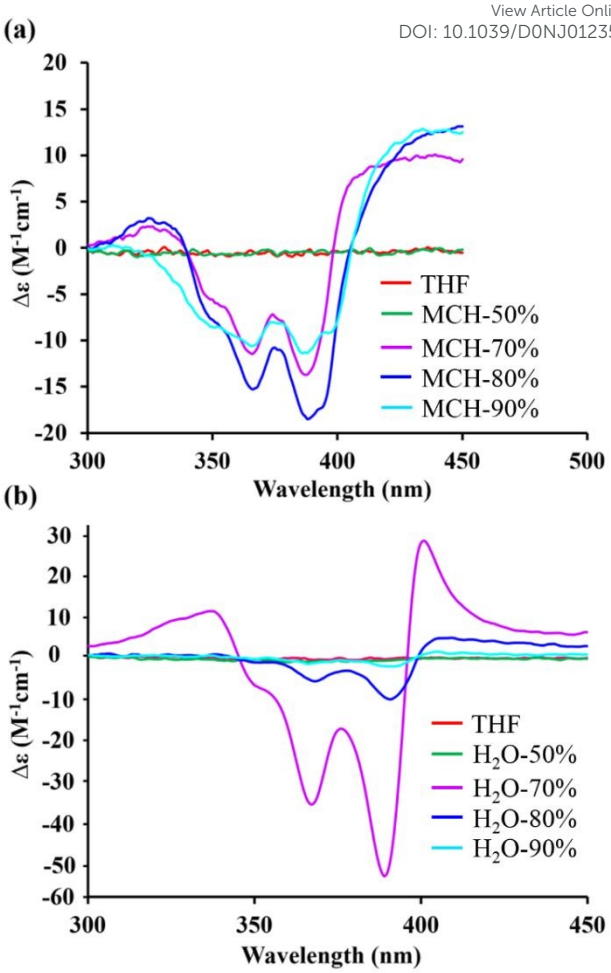

Fig.8 Circular dichroism (CD) spectra of NDI-LCA in (a) THF, THF:MCH and (b) THF and THF:H_2O, respectively

3.10. Computational properties

The *in vacuo* time-dependent density functional theory (TDDFT) calculations were conducted using the ORCA 4.0 suit of programs.[42] Initially the molecular structures were geometry optimized, then TDDFT calculations were carried out using the B3LYP def2-TZVP basis set. Gauss-Sum 3.0 program[43]and Avogadro version 1.2.0 [44] were used to build the molecular structures and process the results of ORCA calculations.

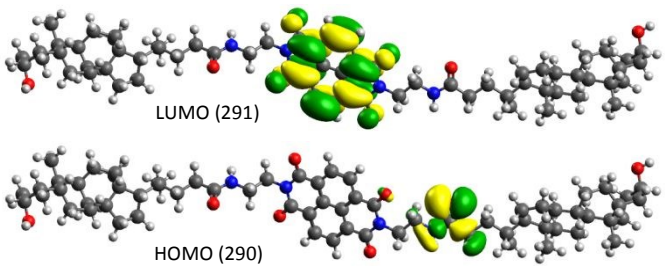

Fig.9 Frontier molecular orbitals HOMO and LUMO wave function of NDI-Lithiocholamide as calculated using TDDFT at B3LYP/def2-TZVP basis set.

View Article Online
DOI: 10.1039/D0NJ04275A

The calculations showed a LUMO concentrated on the NDI core for NDI-LCA, while the HOMO of NDI-LCA is concentrated on the amide linker moieties to LCA (Fig.9). The calculated HOMO and LUMO energy levels were -6.731eV and -3.980 eV (HOMO–LUMO gap 2.751 eV) (see Fig.9). The HOMO→LUMO transition obtained using theoretical calculations at 518.85 nm gave a very weak oscillation strength that means low charge transfer transitions, the simulated density of state (DOS), UV-vis, and CD spectra are shown in Fig.S12, in which CD shows right-handed helical conformation.

3.11. Mechanism of assembly formation

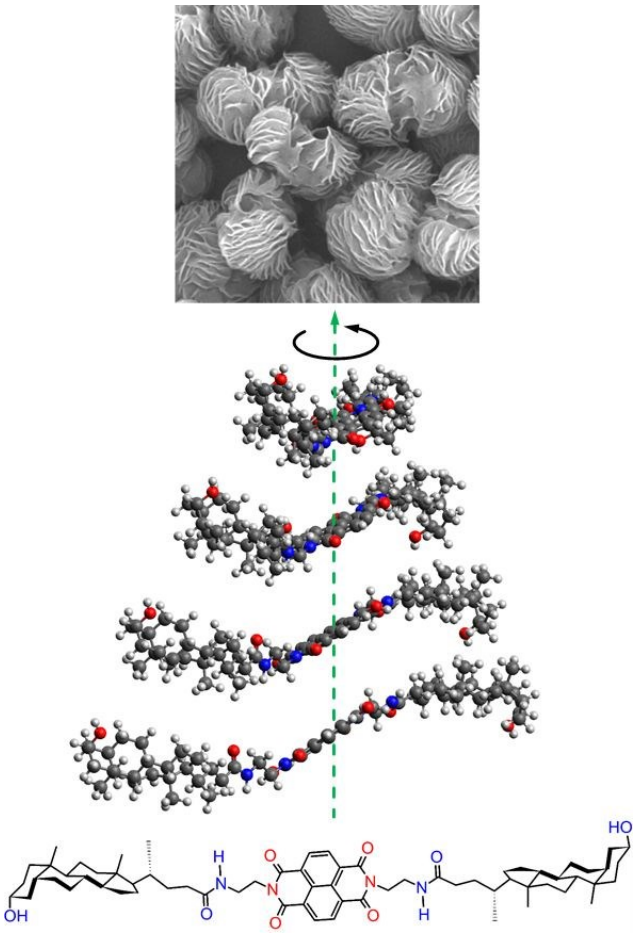

Fig. 10 Schematic presentation of chiral globular cocoon-like microstructures.

As illustrated in Fig.10, the mechanism of formation of chiral flower may involve (i) intermolecular π-π stacking interaction between NDI cores; (ii) hydrophobic interaction between the LCA core; (iii) amide hydrogen bonding, and (iv) H-bonding between –OH group of one molecule faces to other, which is in close proximity. The chirality in flower-like nanostructure is induced from the LCA chiral centres via molecular packing with a non-zero angle concerning the nearest molecular scaffolds, which induces the chiral twist and leading to the chiral flower morphology. The mechanism based on the obtained CD spectra as well as supramolecular assembly nanostructures revealed by SEM demonstrate right-handed helical structures, size of the helicity decreases with increasing H_2O content beyond 80%, the NDI-LCA shows flattening the CD curve (Fig. 8) and obtained fibril structures (ESI Fig. 8), indicating loss of chirality in higher %'s of a polar solvent. These results are similar to an earlier report by Wei and co-workers for helical structures of PANI:$_S$-CSA and PANI:$_R$-CSA.[45,46]

3.12. Cytotoxicity assay

The cytotoxicity of the synthesized NDI-LCA and NDI (ESI†, Scheme S1) was performed in Neuro-2a murine cancerous cells by in vitro MTT assay at various concentrations. It was observed that NDI-LCA had above 80% of cell viability upto as higher as 50µg/100µL concentration as shown in Figure 11. Therefore, NDI-LCA was found to be more bio-compatible[48] exhibiting dose-dependent cytotoxicity at very high concentrations compared to its counterpart NDI (ESI†, Scheme S1).

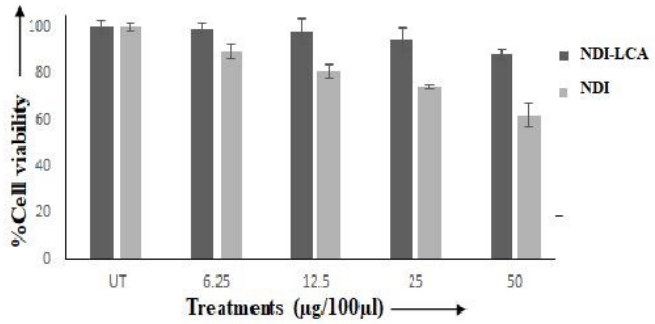

a.

Fig. 11 Comparative cell viability study of NDI-LCA & NDI on Neuro-2a murine cancerous cells at different concentrations (24 h).

3.13. Intra-cellular morphology & uptake study:

The Neuro-2a cells were treated with NDI-LCA and NDI (ESI†, Scheme S1) at 10µg/100µl concentration and observed for cellular morphology and uptake by using a fluorescence confocal microscope as displayed in Figure 12. It was visibly observable that there was no effective change in the morphology of the Neuro-2a cells after the above treatments compared to the control (untreated- UT) Neuro-2a cells. From the images, it can be comprehended that the NDI-LCA and the Lyso Tracker Red (LTR) standard are co-localized at similar cellular regions at the time points (3hr, 6hr, and 24hrs) more specifically than the ones treated with NDI. The blue fluorescence of NDI-LCA and NDI (ESI†, Scheme S1) were found to be stable even until the 24 h time-point. These observations noticeably connote the bio-compatible nature and operative application of NDI-LCA as a fluorescence tracker and delivery agent upon future studies.

View Article Online
DOI: 10.1039/D0NJ01235A

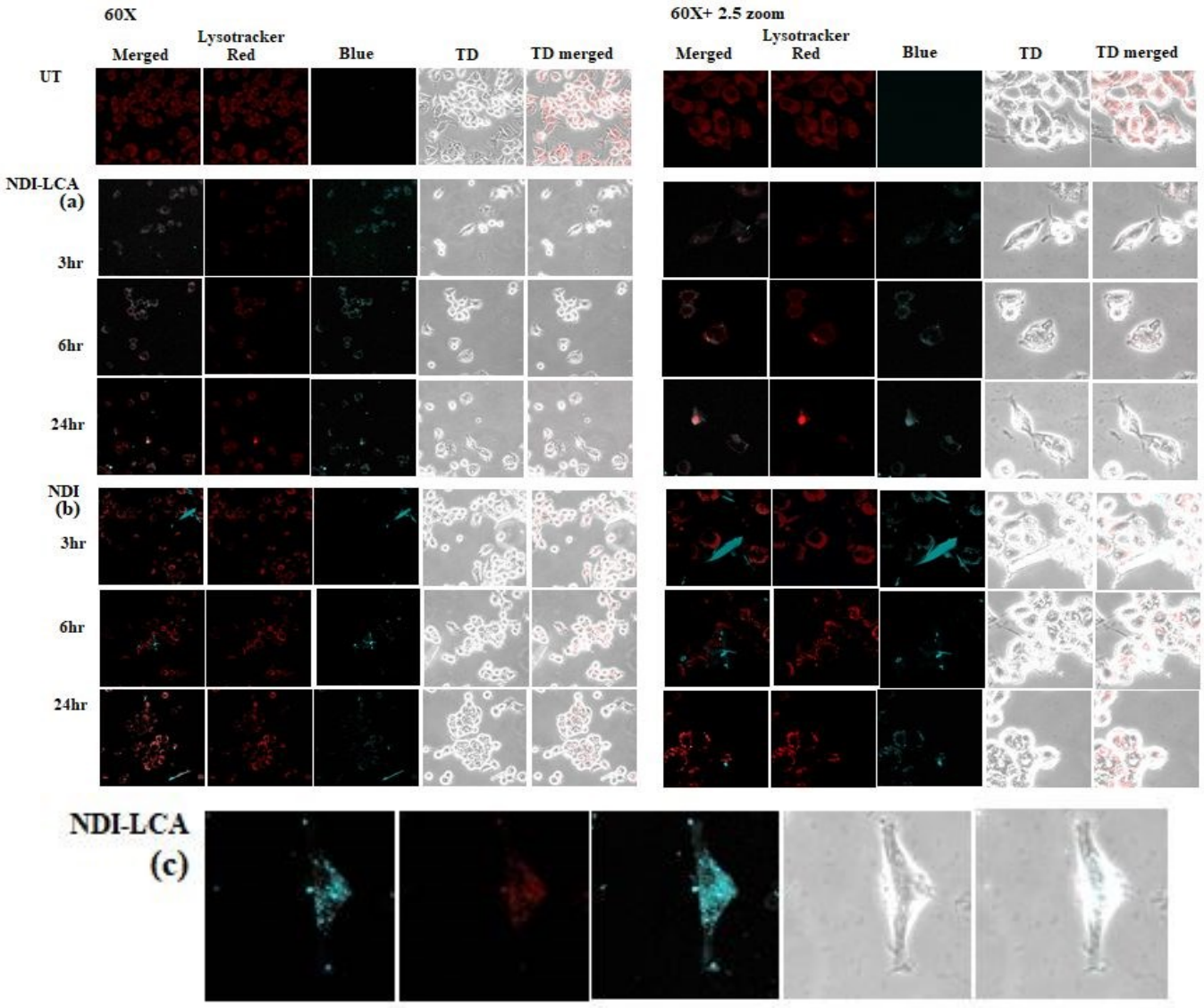

Fig. 12 Confocal images of fixed Neuro-2a murine cancerous cells incubated with (a) NDI-LCA, (b) NDI and LysoTracker Red) at 60X magnification (scale 10µm and 2.5zoom) and time points (3h, 6h and 24h). (c) Single cell 60X+ 3.5 zoom image (NDI-LCA).

4. Conclusions

In summary, we designed and synthesized naphthalenediimide-lithocholic acid conjugate. Here, the NDI-LCA undergoes chiral flower-like morphology formation in THF:MCH, (2:8 and 3:7, *v/v* ratio). Whereas, in THF:H_2O (3:7, *v/v* ratio), chiral helical nanostructure formation takes place. The chirality is expressed in self-assembled supramolecular flowers and nanostructures were proved by CD spectroscopy techniques. We believe that such chiral nanostructure formation in different solvents could encourage to develop such systems for the fabrication of chiral technological tools. From the cellular toxicity, morphology and uptake analysis, it is evident that the supramolecular structures of NDI-LCA are non-toxic even at higher concentrations towards neuro-2A cells and possess efficient blue fluorescence which can be developed as a cell marker and delivery agent in future drug delivery studies.

Conflicts of interest

The authors declare that "There are no conflicts of interest".

Acknowledgments

S.M.W. acknowledges CSIR for senior research fellowship (SRF). S.V.B. (IICT) is grateful for financial support from The Director CSIR-IICT, Hyderabad, India under the P07 project and IICT/Pubs./2020/081. S.V.B. (GU) acknowledge financial support and Professorship from the UGC-FRP. N. Puvvada acknowledge DST-Inspire faculty scheme for the financial support.

Notes and R**eferences**

1 J.-M. Lehn, Supramolecular Chemistry: Concept and Prespectives (VCH, Weinheim), 1995.
2 A. S. Mahadevi and G. N. Sastry, *Chem. Rev*., 2016, **116**, 5, 2775-2825.
3 Y. Wang, J. Xu, Y. Wang and H. Chen, *Chem. Soc. Rev*., 2013, **42**, 2930– 2962.
4 M. Liu, L. Zhang and T. Wang, *Chem. Rev*., 2015, **115**, 7304–7397.
5 R. Breslow, M. Levine and Z.-L. Cheng, *Origins Life Evol. Biosphere*, 2010, **40**, 11.
6 (a) L. Addadi and S. Weiner, *Nature*, 2001, **411**, 753– 755; (b) R. A. Hegstrom and D. K. Kondepudi, *Sci. Am*., 1990, **262**, 108– 115; (c)J. M. Lehn, *Angew. Chem., Int. Ed. Engl*., 1990, **29**, 1304– 1319; (d) T. Aida, E. W. Meijer and S. I. Stupp, *Science*, 2012, **335**, 813–817.
7 W. L. Noorduin, A. Grinthal, L. Mahadevan and J. Azenberg, *Science*, 2013, **340**, 832-837.
8 R. M. Erb, H. S. Son, B. Samanta, V. M. Rotello and B. B. Yellen, *Nature*, 2009, **457**, 999-1002.
9 J. Ge, J. Lei and R. N. Zare, *Nat. Nanotechnol*., 2012, **7**, 428-432.
10 X. F. Shen and X. P. Yan, *Angew. Chem. Int. Ed*., 2007, **46**, 7659-7663.
11 C. K. King'ondu, A. Iyer, E. C. Njagi, N. Opembe, H. Genuino, H. Huang, R. A. Ristau and S. L. Suib, *J. Am. Chem. Soc*., 2011, **133**, 4186-4193.
12 S. Xiong, J. S. Chen, X. W. Lou, H. C. Zeng, *Adv. Funct. Mater*., 2012, **22**, 861-871.
13 T. Nakanishi, K. Ariga, T. Michinobu, K. Yoshida, H. Takahashi, T. teranishi, H. Möhwald and D. G. Kurth, *Small*, 2007, **3**, 2019-2023.
14 Y. Liu, X. Ji and Z. He, *Nanoscale*, 2019, **11**, 17179-17194.
15 S. W. Lee, S. A. Cheon, M. I. Kim and J. J. Park, *J. Nanobiotechnol.,* 2015, **13**, 54.
16 J. Hu, G. Liu and G. Nijkang, *J. Am. Chem. Soc*., 2008, **130**, 3236-3237.
17 G. Zhu, R. Hu, Z. Zhao, Z. Chen, X. Zhang, and W. Tan, *J. Am. Chem. Soc*., 2013, **135**, 16438-16445.
18 R. W. Jadhav, D. D. La, V G. More, H. T. Vo, D. A. Nguyen, D. L. Tran and S. V. Bhosale, *Sci. Rep*., 2020, **10**, 154.
19 N. Berova, K. Nakanishi and R. W. Woody, Circular dichroism: principles and applications, 2nd ed.; Wiley-VCH: New York, 2000.
20 L. D. Barron, Molecular light scattering and optical activity; Cambridge University Press: New York, 2004.
21 W. Feng, J.-Y. Kim, X. Wang, H. A. Calcaterra, Z. Qu, L. Meshi and N. A. Kotov, *Sci. Adv*., 2017, **3**, e1601159.
22 W. Jiang, M. S. Pacella, D. Athanasiadou, V. Nelea, H. Vali, R. M. Hazen, J. J. Gray and M. D. McKee, *Nat. Commun*., 2017, **8**, 15066.
23 T. Nakanishi, T. Michinobu, K. Yoshida, N. Shirahata, K. Ariga, H. Mohwald and D. G. Kurth, *Adv. Mater*., 2008, **20**, 443–446
24 M. Salimimarand, D. D. La, M. Al Kobaisi and S. V. Bhosale, *Sci. Rep.,* 2017, **7**, 42898
25 Y. Duan, X. Liu, L. Han, S. Asahina, D. Xu., Y. Cao, Y. Yao and S. Che, *J. Am. Chem.Soc.,* 2014, **136**, 7193-7196.
26 W. H. Pirkle and T. C. Pochapsky, *J. Am. Chem. Soc.,*1987, **109**, 5975-5982
27 H. J. Davis and R. J. Phipps, *Chem. Sci.,* 2017,**8**, 864-877
28 (a) T. J. ward and D.-M. Hamburg, *Anal. Chem*.,2004, **76**, 4635-4644; (b) T. J. Ward and K. D. Ward, *Anal. Chem*.,2012, **84**, 626-635; (c) C. Fernandes, M. E. Tiritan and M. M. M. Pinto, *Symmetry*, 2017, **9,** 206.
29 W. H. Brooks, W. C. Guida and K. G. Daniel, *Curr. Top. Med.Chem.,* 2011, **11**, 760–770.
30 D. W. Green, J.-M. Lee, E.-J. Kim, D.-J. Lee and H.-S. Jung, *Adv. Mater. Interface*, 2016, **3**, 1500411.
31 (a) Y. Dong, Y. Zhang, X. Li, Y. Feng, H. Zhang and J. Xu, *Small*, 2019, **15**, 1902237; (b) X. Shang, I. Song, J. H. Lee, M. Han, J. C. Kim, H. Ohtsu, J. Ahn, S. K. Kwak and J. H. Oh, *J. Mater.Chem. C*, 2019, **7**, 8688-8697; (c) E. Yashima, N. Ousaka, D. Taura, K. Shimomura, T. Ikai and K. Maeda, *Chem. Rev.,* 2016, **116**, 13752–13990
32 (a) P. K. Endress, *Curr. Opin. Plant Biol.*, 2001, **4**, 86-91; (b) F. Zsila, J. Deli and M. Simonyi, *Planta*, 2001, **213**, 937-942; (c) ; (d)
33 D. M. Small, The Bile Acids, in Chemistry, Physiology and Metabolism, ed. P. P. nairand D. Kritchevsky, Plenum Press, New York. 1971.
34 S. Mukhopadhyay, U. Maitra, *Curr. Sci.,* 2004, **87**, 166-1683.
35 (a) D. M. Small, *Adv. Chem. Ser*., 1968, **84**, 31-53; (b) P. Terech, S. K. P. Velu, P. Pernot and L. Wiegart, *J. Phys. Chem. B*, 2012, **116**, 11344-11355; (c) P. Terech and Y. Talmon, *Langmuir*, 2002, **18**, 7240-7244; (d) P. Terech, A. de Geyer, B. Struth and Y. Talmon, *Adv. Mater*., 2002, **14**,495-498; (e) U. Maitra and A. Chakrabarty, *Beilstein J. Org.Chem*., 2011, **7**, 304-309; (f) X. Zhang, J. Zou, K. Tamhane, F. F. Kobzeff and J. Fang, *Small*, 2010, **6**, 217-220; (g) A. Pal, H. basit, S. Sen, V. K. Aswal and S. Bhattacharya, *J. Mater. Chem*., 2009, **19**, 4325-

View Article Online
DOI: 10.1039/D0NJ01235A

4334; (h) B. Jean, L. Oss-Ronen, P. Terech and Y. Talmon, *Adv. Mater*., 2005, **17**, 728-731.
36 (a) X. Zhan, K. Tamhane, T. Bera and J. Fang, J. Mater. Chem., 2011, 21, 13973-13977; (b) P. Terech, N. M. Sangeetha, S. Bhat, J.J. Allegraud and E. Buhler, *Soft Matter*, 2006, **2**, 517-522.
37 M. A. Kobaisi, S. V. Bhosale, K. Latham, A. M. Raynor and S. V. Bhosale,*Chem. Rev*.,2016, **116**, 11685-11796
38 (a) G. D. Pantos, P. Pengo, and J. K. M. Sanders, *Angew. Chem., Int. Ed.,* 2007, **46**, 194– 197; (b) S. P. Goskulwad, M. A. Kobaisi, D. D. la, R. S. Bhosale, M. Ratanlal, S. V. Bhosale and S. V. Bhosale, *Chem. Asian J*., 2018, **13**, 3947-3953; (c) M. Pandeeswar, M. B. Avinash and T. Govindaraju, *Chem. Eur. J*., 2012, **18**, 4818-4822; (d) F. Salerno, J. A. Berrocal, A. T. Haedler, F. Zinna, E. W. Meijer and L. Di Bari, J. Mater. Chem. (e)
C, 2017, **5**, 3609-3615. (f) A. Sikder, J. Sarkar, R. Barman, and S. Ghosh*, J. Phys. Chem. B 2019, 123, 33, 7169–7177.
39 S. M. Wagalgave, S. D. Padghan, M. D. Burud, M. Al Kobaisi, D. D. La, R. S. Bhosale, S. V. Bhosale and S. V. Bhosale, *Sci. Rep*., 2020, **9**, 12825.
40 M. B. Avinash, E. Verheggen, C. Schmuck and T. Govindaraju, *Angew. Chem. Int. Ed.*, 2012, **51**, 10324-10328.
41 A. T. R. Williams, S. A. Winfield and J. N. Miller, *Analyst* 1983, **108**, 1067–1071.
42 F. Neese, The ORCA program system. *WIREs: Comput. Mol. Sci.,*2012**,2**, 73.
43 N. M. O'boyle, A. L. Tenderholt and K. M. Langner, *J. Comput. Chem.,* 2008**,29**, 839.
43 M. D. Hanwell, D. E. Curtis, D. C. Lonie, T. Vandermeersch, E. Zurek and G. R. Hutchison, *J. Cheminformatics* 2012**,4**, 17.
44 J. V. Selinger, F. C. MacKintosh and J. M. Schnur, *Phys. Rev. E*,
1996, **53**, 3840.
45 Y. Yang, J. Liang, F. Pan, Z. Wang, J. Zhang, K. Amin, J. Fang, W. Zou, Y. Chen, X. Shi and Z. Wei, *Nat. Commun*., 2018, **9**, 3808.46.
46. Y. Yang, Y. Zhang and Z. Wei, *Adv. Mater*., 2013, **25**, 6039.
47 P. Mukherjee, A. Kumar, K. Bhamidipati, N. Puvvada, and S.K. Sahu*, ACS Appl. Bio Mater. 2020, 3, 2, 869–880.
48. Puvvada, N.; Kumar, B. N.; Konar, S.; Kalita, H.; Mandal, M.; Pathak, A., Sci Technol Adv Mater 2012, **13 (4)**, 045008.

View Article Online
DOI: 10.1039/D0NJ01235A

Graphical abstract